Search for axions from the 1115-keV transition of ^{65}Cu

F. T. Avignone III,[2] C. Baktash,[3] W. C. Barker,[2] F. P. Calaprice,[1] R. W. Dunford,[1]*
W. C. Haxton,[4] D. Kahana,[1] R. T. Kouzes,[1] H. S. Miley,[2] D. M. Moltz[2]†

[1]*Princeton University, Princeton, New Jersey 08544*
[2]*University of South Carolina, Columbia, South Carolina 29208*
[3]*Oak Ridge National Laboratory, Oak Ridge, Tennessee 37830*
[4]*University of Washington, Seattle, Washington 98195*

(Received 16 July 1987)

Two independent axion searches have been carried out near a well-shielded radioactive ^{65}Zn source (~ 15 kCi). One experiment used four NaI(Tl) scintillators to detect coincident photons generated in the decay $a \rightarrow \gamma\gamma$. The second used a shielded 145-cm^3 low-background intrinsic-Ge detector to detect single photons produced by axion "Compton" interactions with detector electrons and by Primakoff conversion off Ge nuclei and off Pb nuclei in the detector shield. We determine general constraints imposed by these experiments on axions that couple to nucleons and to either the electron or two photons. In the case of light axions, the limits obtained in the second experiment are new. For the standard axion, we determine the ranges of f_ϕ and X that are ruled out by our measurements.

I. INTRODUCTION

One elegant solution to the strong CP problem, the apparent weakness of the P- and CP-violating term in the QCD Lagrangian, was proposed some time ago by Peccei and Quinn[1] (PQ). Their solution, the imposition of a global chiral U(1) symmetry on the world Lagrangian, implies the existence of a light neutral pseudoscalar, the axion.[2] However, despite many careful searches for axions in beam-dump, reactor, and nuclear-decay experiments, this particle has so far eluded discovery.

Although the original axion, associated with PQ symmetry breaking at the weak scale, is ruled out by experiment, many variant PQ models and their associated axions are still viable. If the scale of the PQ symmetry breaking is made very large, the mass and couplings of the axion are proportionately reduced, and experimental detection becomes difficult. Cosmological and astrophysical arguments[3] would appear to restrict the masses of such "invisible" axions to the rather narrow 10^{-2} eV $\gtrsim m_a \gtrsim 10^{-5}$ eV range. Composite invisible axions have been proposed that, unlike the standard axion, lack couplings to heavy quarks and to leptons, and may have suppressed decay rates into two photons.[4] More recently, motivated in part by the curious e^+e^- pairs produced in heavy-ion collisions, variant axion models have been constructed where the PQ symmetry breaking occurs at or below the weak scale.[5] Such models circumvent most (but not all[6]) of the experimental constraints by requiring the axion to decay rapidly into e^+e^- and to couple very weakly to heavy quarks.

It is apparent that reasonable theoretical models can lead to axions with very different masses, couplings, and lifetimes. Experiments probing distinct properties of axions, even if redundant in the context of a particular model, provide independent constraints on theories in-

corporating the PQ symmetry. In the present paper we present some new constraints on the couplings of light axions to nucleons.

We have undertaken two independent searches for axions emitted from a well-shielded ~ 15-kCi ^{65}Zn source. This source feeds the $\frac{5}{2}^-$ excited state in ^{65}Cu that may decay to the ground state by emitting an axion with a total energy of 1115 keV (see Fig. 1). In the first experiment we attempted to detect the photons from the in-flight decay $a \rightarrow \gamma\gamma$ of the emitted axion. The signal was a coincidence between any two of the four NaI(Tl) detectors. We note that this experiment is very similar to the earlier ^{65}Cu experiment performed by Lehmann et al.[7] who achieved a lower background rate but used a weaker source. In the second, we searched for evidence of direct conversion of an axion into a photon in the spectrum obtained from a low-background intrinsic-Ge detector. The two processes of interest in the second experiment are Primakoff production off the Ge nuclei and axion "Compton" production off the electrons in the detector. If the photon produced in either of these processes is fully absorbed in the detector, the result is a monoenergetic line at the transition energy (1115 keV).

The first experiment tests the product of the axion's couplings to the nucleon and to two photons. The phase space for the decay $a \rightarrow \gamma\gamma$ depends on m_a^3, and the $a \rightarrow \gamma\gamma$ coupling is expected to be proportional to m_a. Because of this m_a^5 dependence of the $a \rightarrow \gamma\gamma$ decay width, the experiment is rendered insensitive to light axions: In the proper frame, an axion with $m_a = 100$ keV will live approximately 100 times longer than one with $m_a = 250$ keV. Once the axion decay length exceeds the experimental flight path, the experimental sensitivity is diminished accordingly. However, the Primakoff amplitude is also governed by the axion-$\gamma\gamma$ coupling, and the phase space for this process increases with decreasing
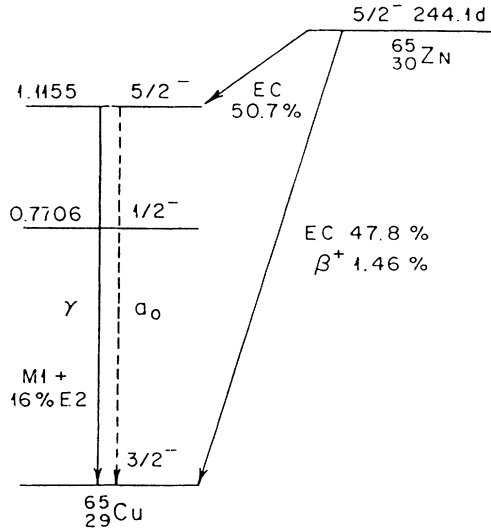
FIG. 1. Decay of ^{65}Zn radioactive source and partial level diagram for ^{65}Cu. The 1115-keV level normally decays by $M1$ γ emission, but if the axion (a_0) exists, it can also decay via axion emission (dashed line).

FIG. 2. Experimental layout showing the ^{65}Zn source, lead shielding, and detectors used in the axion searches.

m_a. Thus the second experiment provides an attractive alternative to the first in the region of small m_a. Similarly, because the Compton phase space is approximately independent of m_a for small m_a, the second experiment also permits us to place constraints on the product of the axion-nucleon and axion-electron couplings for light axions. The relative insensitivity of the detection reactions to the axion mass underscores the power of the high-resolution, low-background, singles-counting technique.

In Sec. II we discuss the design of the two experiments, describing in some detail the ^{65}Zn source, the data-acquisition system and the intrinsic-Ge and NaI detectors. In Sec. III the nuclear axion-decay rate is written in terms of the γ-decay rate, the isoscalar and isovector axion-nucleon couplings, and two ratios of nuclear matrix elements. Shell-model calculations that we performed to estimate these ratios are described in Sec. IV. Rather detailed calculations of the electromagnetic properties of low-lying states in ^{65}Cu are presented to determine the reliability of the wave functions. In Sec. V we discuss the axion-detection reactions, the dependence of the Primakoff and Compton cross sections on the axion mass, and the screening corrections that enter for small m_a. Finally, in Sec. VI, we present our results. Our limits are presented both as general constraints on the couplings of light pseudoscalar bosons and, for the standard axion, as constraints on the Peccei-Quinn scale f_ϕ and the ratio X of the vacuum expectation values of the Higgs fields.

II. EXPERIMENTAL ARRANGEMENT

A. ^{65}Zn source

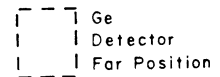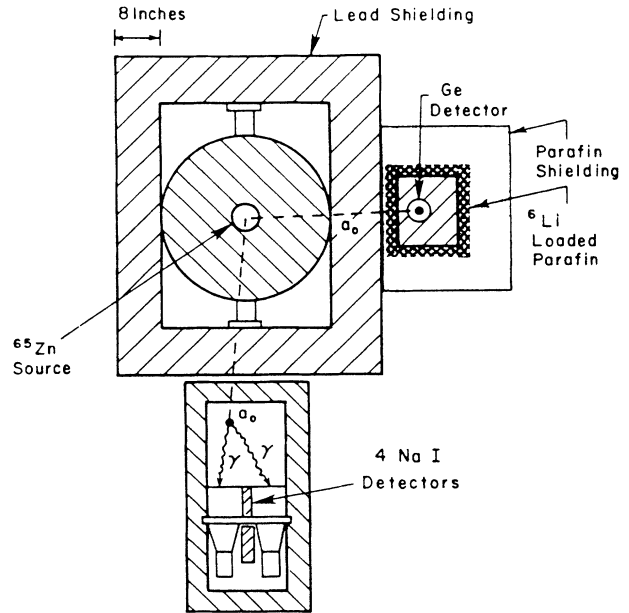The experiments were carried out in the Trans-Uranic Research Building at the Oak Ridge National Laborato-

ry. A schematic diagram of the experimental layout is given in Fig. 2. The radioactive ^{65}Zn source was prepared by exposing eight cylinders of zinc in the Oak Ridge High Flux Reactor. The cylinders, measuring 5.64 cm in diameter and 7.94 cm in length, had an average mass of 77.95 g. Six of the slugs were assembled in a close-packed configuration and sealed by welding in a steel can 14 cm in diameter and 16.5 cm in length. The average activity, determined by measuring the activities of small zinc plates that had been placed between the slugs during exposure, was approximately 15.5 kCi during the NaI experiment and 10.9 kCi during the Ge experiment.

The steel cylinder containing the source was placed inside a large square lead shield assembled so as to avoid direct line-of-sight cracks. There were six layers of lead bricks between the source and the outside of the shield. Accounting for the cavity containing the source, there was a minimum of 54 cm of lead between the source and the outer surface of the shield. The theoretical attenuation factor for the shield is 5.8×10^{-18} for 1115-keV γ rays.

In addition, each detection system was surrounded by its own lead shield, providing an additional 10 cm (8 cm) of lead between the source and the Ge detector (NaI detectors). The resulting total attenuation factors were 4×10^{-21} and 2×10^{-20}, respectively, for the Ge and NaI detectors.

B. Ge detector

The high-resolution, 145-cm^3 intrinsic coaxial Ge detector was mounted in a special low-background cryostat. The detector and cryostat were purchased from the PGT Corporation, Princeton, New Jersey. The detector was shielded, on sides away from the source, by 20.3 cm of lead, with the innermost bricks made of 200-yr-old lead. These were later replaced with virgin lead from Doe-Run mine in St. Joseph, Missouri, but no significant difference in background was observed. The lead was surrounded on all four sides and on top with Li-loaded paraffin and ordinary paraffin of varying thickness (averaging about 15 cm). The cryostat and each lead brick were washed carefully with detergent and water, and then with distilled alcohol. These cleaning precautions removed a slight ^{65}Zn contamination that had been detected in the early phases of the experiment. The data-acquisition system consisted of a spectroscopy amplifier and a 8192-channel pulse-height analyzer. No special electronic stabilization was used.

The stability of the data-acquisition system, as well as the energy resolution and line shape, was monitored continuously by summing all of the data for the peak at 1001.03 keV. This peak is a well-known background γ ray from the decay of ^{234}Pa. The combined data for this peak have a full width at half maximum of 2.47 keV. The energy calibration was accomplished with the well-known background lines at 511.01, 583.14, 911.07, 967.97, 1001.03, and 1460.75 keV. From the calculated slope of the energy calibration curve and the channel number of the 1001.03-keV γ-ray peak, we determined the channel for the 1115.5-keV axion signal. In this way, the location of the potential peak for axions was determined to within a few tenths of a channel. This accuracy is much better than can be obtained by periodic calibrations with radioactive sources. In addition, this procedure properly accounts for all gain shifts and channel-zero shifts throughout the entire experiment.

Several attempts were made to reduce the background to the lowest level possible. Most of the background lines were due to contamination in the aluminum vacuum cap and heat shield surrounding the detector, in the electronic components, and in the stainless-steel tubes and flanges.[8] The intensities of the 139.68-keV γ-ray line in ^{75}Ge and the 198.60-keV line in the daughter nucleus ^{75}As, comparable to those from radioactive contamination, indicated a significant neutron background. The most plausible source is the capture of moderated neutrons on ~37% abundant ^{74}Ge. A significant flux of energetic neutrons can also produce ^{75}Ge by $(n,2n)$ reactions on 7.67% abundant ^{76}Ge. In any case, it was determined that the presence of neutrons, either from cosmic-ray reactions or other sources in the building, was the limiting factor in further lowering the background.

Initially, with the detector located 74.9 cm from the source, data were taken over several counting periods of 10 to 30 days duration, for a total of 83.3 days. The detector, lead shield, and neutron shielding were then mounted on wheels, moving the detector to a distance of 101.8 cm from the source. Data collection continued for an additional 211.5 days. The average source strengths at the first and second positions were 17.1 and 8.4 kCi, respectively. Periodically, during the second phase of the experiment, the detector was wheeled to a third distance, 320 cm away from the source, a position selected to change the solid angle intercepted by the detector by a factor of 10. A limited amount of data (65 days at an average source strength of 10.0 kCi) was collected as a check on background rates. These data, which showed no evidence that the background varied with position, are not included in our analysis.

C. NaI detectors

We searched for the decay of an axion into two gamma rays with an array of four 10.16 cm × 12.7 cm NaI(Tl) detectors. The shielding configuration and 40-cm decay region (Fig. 2) were suitable for detecting axions with masses in the range 150–1100 keV. The signature of an axion event is a coincidence between any pair of the four NaI detectors having a total energy of 1115 keV. Low-background lead filled the 5-cm gap between detectors, and the whole NaI assembly was surrounded by a box with 8-cm lead walls lined with copper. Plastic scintillator paddles above and below the box served as a cosmic-ray anticoincidence shield. Unlike the experiment of Lehmann et al.,[7] no scintillator was used between the NaI(Tl) detectors.

A complete description of the electronics for this experiment is given in Ref. 9. The data-acquisition system was designed around an Apple microcomputer and a CAMAC system. A control program running on the Apple handled the accumulation and storage of data on floppy disk.

The control program polled CAMAC for data available from the four NaI detectors. The analog-to-digital converter (ADC) was gated by a requirement of any pair of NaI triggers. If the ADC data passed software energy cuts, they were dumped to a floppy disk for later processing. In addition, every 12 hours singles spectra were accumulated for a weak ^{137}Cs source placed near the detectors. These calibrations verified the detector gain stability over the many months of data acquisition. Intermittently, a ^{22}Na source was used to test the system pair efficiency.

A total of 54.3 days of data was taken. During the experiment the source activity diminished from 20.3 kCi to 11.1 kCi, with 15.5 kCi the average value.

III. NUCLEAR AXION DECAY

We consider the decay of the 1115 keV $\frac{5}{2}^-$ state in ^{65}Cu to the $\frac{3}{2}^-$ ground state via axion emission, a process that competes with ordinary $M1$ and $E2$ gamma decay. The levels are shown in Fig. 1. This decay is somewhat more complicated than others that have been considered owing to the strong orbital contribution to the $M1$ decay.

The coupling of the axion field ϕ_a to the nucleon field $\psi_N = \binom{p}{n}$ can be written

$$\mathcal{L}_{\text{eff}} = i\bar{\psi}_N \gamma_5 (g^0_{aNN} + g^1_{aNN}\tau_3)\psi_N \phi_a \ . \tag{1}$$

Axion-decay transitions are thus sensitive to isoscalar and isovector transition densities, if both g^0_{aNN} and g^1_{aNN} are nonzero. The nuclear axion-decay rate is easy to evaluate with conventional techniques,[10] yielding, for an $M1$ transition in the long-wavelength limit,

$$\omega_a = \frac{1}{24\pi} \frac{k_a^3}{M^2} \frac{1}{2J_i+1} \left| \left\langle J_f \left| \left| \sum_{i=1}^{A} [g^0_{aNN} + \tau_3(i)g^1_{aNN}]\sigma(i) \right| \right| J_i \right\rangle \right|^2 , \tag{2}$$

where k_a is the three-momentum of the outgoing axion, M is the nucleon mass, J_i and J_f are the initial and final nuclear angular momenta, and $\sigma(i)$ is the nuclear spin operator. The nuclear matrix element appearing in Eq. (2) is reduced in angular momentum.

The corresponding gamma decay rate is

$$\omega_\gamma = \frac{\alpha}{12} \frac{k^3}{M^2} \frac{1}{2J_i+1}(1+\delta^2) \left| \left\langle J_f \left| \left| \sum_{i=1}^{A} \{ [\mu_0 + \mu_1\tau_3(i)]\sigma(i) + [1+\tau_3(i)]l(i) \} \right| \right| J_i \right\rangle \right|^2 , \tag{3}$$

where k is the photon three-momentum, δ is the $E2/M1$ mixing ratio, $l(i)$ is the orbital angular momentum operator, and $\mu_0 = \mu_p + \mu_n = 0.88$ and $\mu_1 = \mu_p - \mu_n = 4.71$ are the isoscalar and isovector nuclear magnetic moments, respectively, in nuclear magnetons. As the total angular momentum operator has no off-diagonal matrix elements (and therefore cannot cause transitions),

$$\left\langle J_f \left| \left| \sum_{i=1}^{A} \sigma(i) \right| \right| J_i \right\rangle = -2 \left\langle J_f \left| \left| \sum_{i=1}^{A} l(i) \right| \right| J_i \right\rangle ,$$

so that the isoscalar orbital operator can be eliminated. Thus

$$\omega_\gamma = \frac{\alpha}{12} \frac{k^3}{M^2} \frac{1}{2J_i+1}(1+\delta^2) \left| \left\langle J_f \left| \left| \sum_{i=1}^{A} \{ [\mu_0 - \tfrac{1}{2} + \mu_1\tau_3(i)]\sigma(i) + \tau_3(i)l(i) \} \right| \right| J_i \right\rangle \right|^2 . \tag{4}$$

Note that the isoscalar spin contribution to ω_γ is often extremely weak because of the small coupling $(\mu_0 - \tfrac{1}{2}) \approx 0.38$.

We define two nuclear-structure-dependent ratios

$$\eta = -\frac{\left\langle J_f \left| \left| \sum_{i=1}^{A} l(i)\tau_3(i) \right| \right| J_i \right\rangle}{\left\langle J_f \left| \left| \sum_{i=1}^{A} \sigma(i)\tau_3(i) \right| \right| J_i \right\rangle} \tag{5}$$

and

$$\beta = \frac{\left\langle J_f \left| \left| \sum_{i=1}^{A} \sigma(i) \right| \right| J_i \right\rangle}{\left\langle J_f \left| \left| \sum_{i=1}^{A} \sigma(i)\tau_3(i) \right| \right| J_i \right\rangle} . \tag{6}$$

Once the axion isoscalar and isovector couplings to nucleons are fixed, the axion decay rate is determined by ω_γ and these ratios. The resulting axion-to-gamma decay-rate ratio is

$$\frac{\omega_a}{\omega_\gamma} = \frac{1}{2\pi\alpha} \left[\frac{k_a}{k} \right]^3 \frac{1}{1+\delta^2} \left[\frac{g^0_{aNN}\beta + g^1_{aNN}}{(\mu_0 - \tfrac{1}{2})\beta + (\mu_1 - \eta)} \right]^2 . \tag{7}$$

The partial half-life of the 1115-keV state [0.26 psec (Ref. 11)] and the mixing ratio [$\delta = 0.44 \pm 0.02$ (Ref. 12)] are known. Thus the nuclear-structure uncertainties enter only in estimating η and β.

The axion-nucleon coupling strengths depend on the details of the theory implementing the PQ mechanism. For the standard axion[10] characterized by the PQ scale f_ϕ,

$$g_{aNN}^0 = -\frac{M}{f_\phi}\left[\frac{N-1}{2}\right]\left[X+\frac{1}{X}\right]F_A^0 \ , \tag{8a}$$

$$g_{aNN}^1 = \frac{M}{f_\phi}\left\{\frac{X}{2}\left[1-N\left[\frac{1-Z}{1+Z}\right]\right]\right.$$

$$\left. -\frac{1}{2X}\left[1+N\left[\frac{1-Z}{1+Z}\right]\right]\right\}F_A^1$$

$$\approx \frac{M}{f_\phi}\left[\frac{X}{2}(1-0.28N)-\frac{1}{2X}(1+0.28N)\right]F_A^1 \ , \tag{8b}$$

where X is the ratio of vacuum expectation values for the two PQ Higgs fields and N is the number of quark doublets. The value of the quark mass ratio $Z=m_u/m_d$ used in Eq. (8b) is 0.56. The isovector axial-vector coupling $F_A^1 = -1.26$ while a quark-model estimate predicts $F_A^0 = \frac{3}{5}F_A^1$. The standard axion mass is[2,10]

$$m_a = m_\pi\left[\frac{f_\pi}{f_\phi}\right]N\left[X+\frac{1}{X}\right]\frac{Z^{1/2}}{1+Z}$$

$$\approx 24N\left[\frac{250\text{ GeV}}{f_\phi}\right]\left[X+\frac{1}{X}\right]\text{keV} \ , \tag{9}$$

where $f_\pi \approx 94$ MeV is the pion-decay constant.

IV. NUCLEAR STRUCTURE OF ^{65}Cu

Two shell-model calculations have been made in order to determine wave functions for the low-lying states in ^{65}Cu. In the first a closed ^{56}Fe core was assumed. The nine valence nucleons were restricted to the $2p_{1/2}-2p_{3/2}-1f_{5/2}$ shells, with no other constraints on allowed configurations. The second calculation included in addition the more complicated proton configurations with one hole in the $f_{7/2}$ shell. The inclusion of the spin partner of the $f_{5/2}$ subshell cures a potential deficiency of the first calculation. Each calculation was performed with the full g matrix of Kuo and Brown.[13] The single-particle energy splittings were adjusted in a least-squares fit to the low-lying negative-parity levels in ^{65}Cu. The resulting spectra are shown in Fig. 3. A significant improvement in the agreement with experiment results when excitations of the $f_{7/2}$ shell are included.

One direct test of the wave functions can be made by calculating the electromagnetic properties of the low-lying states in ^{65}Cu. Of particular importance, in the context of our axion experiment, is the reliability of the $M1$ matrix element predictions. The results are shown in Table I. The agreement with experiment is impres-
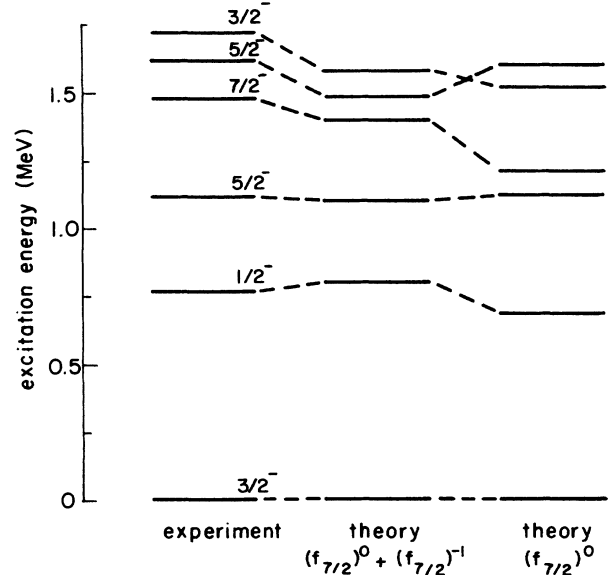

FIG. 3. A comparison of the experimental and shell-model level diagrams for ^{65}Cu. The $(f_{7/2})^0$ calculation assumes a closed $1f_{7/2}$ core, while the $(f_{7/2})^0+(f_{7/2})^{-1}$ calculation permits one-hole excitations of the $1f_{7/2}$ core.

sive. The only significant discrepancy occurs for the $\frac{5}{2}^-$ (1.62 MeV)$\to\frac{3}{2}^-$(0.0 MeV) transition, where $B(M1)$ value is a factor of 2.5 smaller than experiment. However, the experimental value is quite suppressed, so this discrepancy is, in fact, very small in absolute magnitude. The $E2$ strengths, as expected, are systematically underestimated. This operator is highly collective and, unlike the $M1$ operator, can connect to configurations outside of the fp model space. It is satisfying that the inclusion of the $f_{7/2}$-subshell excitations systematically improves the agreement of both the $B(M1)$ and $B(E2)$ values with experiment.

The calculated $B(M1)$ value for the transitions used in the axion search, $\frac{5}{2}^-$ (1.115 MeV)$\to\frac{3}{2}^-$(0.0 MeV), is 0.0449 W.u., compared to the experimental value of 0.0511 W.u. The theoretical mixing ratio, $\delta(E2/M1)=0.35$, is slightly smaller than experiment: 0.44 ± 0.02. Very recently the (e,e') transverse form factor for exciting the $\frac{5}{2}^-$ state was measured for momentum transfers up to 1.3 fm^{-1}. These results are also in good agreement with our theoretical predictions.[14]

For our axion studies we need the two matrix-element ratios η and β. Our shell-model calculations predict $\eta=-6.59$ (-5.86) and $\beta=1.81$ (1.94) for the full (closed $f_{7/2}$ subshell) calculation. The relative sensitivity of our experiment to the isoscalar and isovector axion-nucleon couplings is determined by β: although both couplings contribute, the 1115-keV transition will place stronger constraints on g_{aNN}^0.

How reliable are these calculated ratios? We expect the ratios to be less sensitive to nuclear-physics uncertainties than the absolute $M1$ rates, which, we have seen,

TABLE I. Electromagnetic properties of ^{65}Cu. W.u. denotes Weisskopf units.

$J_i^\pi \to J_f^\pi$	Multipole	$E_i \to E_f$ (MeV)	B^{expt} (W.u.)	B^{theor} (W.u.)[a]	B^{theor} (W.u.)[b]
$\frac{1}{2}^- \to \frac{3}{2}^-$	$M1$	$0.77 \to 0.00$	5.30×10^{-1}	1.25	7.81×10^{-1}
	$E2^c$		1.19×10^1	5.03	9.09
$\frac{5}{2}^- \to \frac{3}{2}^-$	$M1$	$1.12 \to 0.00$	5.11×10^{-2}	8.22×10^{-2}	4.49×10^{-2}
	$E2$		1.31×10^1	2.30	7.48
$\frac{5}{2}^- \to \frac{1}{2}^-$	$E2$	$1.12 \to 0.77$	1.69	9.34×10^{-1}	1.09
$\frac{7}{2}^- \to \frac{3}{2}^-$	$E2$	$1.48 \to 0.00$	1.29×10^1	2.41	6.38
$\frac{7}{2}^- \to \frac{5}{2}^-$	$M1$	$1.48 \to 1.12$	2.16×10^{-1}	4.49×10^{-1}	2.23×10^{-1}
	$E2$		5.38	8.74×10^{-1}	3.45
$\frac{5}{2}^- \to \frac{3}{2}^-$	$M1$	$1.61 \to 0.00$	2.40×10^{-3}	5.75×10^{-3}	9.48×10^{-4}
	$E2$		5.41×10^{-1}	6.01×10^{-3}	7.67×10^{-4}
$\frac{5}{2}^- \to \frac{1}{2}^-$	$E2$	$1.61 \to 0.77$	8.07	2.29	2.82
$\frac{5}{2}^- \to \frac{5}{2}^-$	$M1$	$1.62 \to 1.12$	6.11×10^{-2}	2.00×10^{-1}	6.18×10^{-2}
	$E2$		1.57×10^1	1.16	2.68
$\frac{3}{2}^- \to \frac{3}{2}^-$	$M1$	$1.72 \to 0.00$	$<3.86 \times 10^{-2}$	1.32×10^{-2}	1.84×10^{-2}
$\frac{3}{2}^- \to \frac{1}{2}^-$	$M1$	$1.72 \to 0.77$	$<5.39 \times 10^{-3}$	1.74×10^{-1}	5.03×10^{-2}
$\frac{3}{2}^- \to \frac{5}{2}^-$	$M1$	$1.72 \to 1.12$	$<3.17 \times 10^{-1}$	5.22×10^{-3}	3.94×10^{-1}

[a]Calculated with $2p_{1/2}$-$2p_{3/2}$-$1f_{5/2}$ shell-model wave functions (closed $1f_{7/2}$ shell).
[b]Calculated with full $2p1f$ shell-model wave functions (at most one proton hole is allowed in the $1f_{7/2}$ shell).
[c]All $E2$ matrix elements are calculated with an isoscalar effective charge of $e/2$ added to the bare charge $e/2$.

are well reproduced by theory. It is also comforting that η adds constructively with the isovector magnetic moment in Eq. (7), thus softening the impact of any change in η on the overall rate ω_a. We would consider errors in excess of 30% in either η or β to be highly unlikely.

Using these ratios in Eq. (7) we find

$$\frac{\omega_a}{\omega_\gamma} = 0.13 \left[\frac{k_a}{k} \right]^3 (1.81 g_{aNN}^0 + g_{aNN}^1)^2 . \tag{10}$$

For the case of the standard axion for three generations ($N = 3$) this can be rewritten as

$$\frac{\omega_a}{\omega_\gamma} = 2.9 \times 10^{-6} \left[1 - \frac{m_a^2}{k^2} \right]^{3/2} \left[X + \frac{1.99}{X} \right]^2$$
$$\times \left[\frac{250 \text{ GeV}}{f_\phi} \right]^2 . \tag{11}$$

Thus, the transition is sensitive to both small and large X.

As an example of the expected axion flux, we take $f_\phi \sim 250$ GeV (so that the PQ scale is the weak scale) and set $X = 1$. The standard axion mass [Eq. (9)] would then be 150 keV. It follows that the axion/γ branching ratio is 2.5×10^{-5}. The average ^{65}Zn source strength during the NaI portion of the experiment was 15.5 kCi. Thus approximately 8×10^9 axions would be emitted from the source each second.

V. AXION DETECTION

We now discuss in more detail the reactions that permit us to detect axions. The process studied in the first experiment, $a \to \gamma\gamma$, has the disadvantage that the axion's width in its rest frame is expected to vary as m_a^5. This leads to rapid loss in sensitivity to light axions whose decay length exceeds the experimental flight path. As the opening angle between the γ rays depends on m_a, it is also impossible to optimize the detector configuration without prior knowledge of m_a. These difficulties do not arise in our second experiment, where we exploit the direct interactions of the axion with the electrons and nuclei in the detectors.

The Compton conversion of an axion to a photon can occur off the electrons or the nuclei in the detector. For a neutral atom, the ratio of the electron to nuclear Compton cross sections is given approximately by $(Ze^2/m)/(Z^2e^2/M_A) = M_A/Zm \sim M_N/m$, where m, M_A, and M_N are the electron, nuclear, and nucleon masses, and where the last equality holds exactly for an isoscalar target. Thus Compton conversion off nuclei is quite unimportant. We calculate the Compton conversion amplitude below by treating the bound electrons as quasifree particles.

The Primakoff conversion of an axion to a photon in the Coulomb field of the nucleus is the third process we will consider. The amplitude for this process can be written directly in terms of the $a \to \gamma\gamma$ amplitude. The photon distribution $d\sigma/d\cos\theta$ of the produced photons becomes increasingly forward peaked for small m_a, achieving its maximum at $\theta \sim m_a^2/2\epsilon_a^2$, where m_a and ϵ_a are the mass and energy of the axion. The three-momentum absorbed by the nucleus for this scattering angle is $\sim m_a^2/\sqrt{2}\epsilon_a$. For $\epsilon_a = 1115$ keV, this is ~ 2 keV/c at $m_a = 56$ keV, a momentum comparable to the inverse size of the atom. It is thus apparent that the screening of the nuclear charge by atomic electrons can be important for $m_a \lesssim 50$ keV. This effect is discussed in more detail below.

A. The Primakoff process and $a \to \gamma\gamma$

The one-loop diagram shown in Fig. 4(a) yields an effective amplitude governing the decay $a \to \gamma\gamma$ of the form

$$\mathcal{M}_{a\gamma\gamma} = \frac{\alpha}{\pi}\frac{1}{f_{a\gamma\gamma}}\epsilon^{\mu\nu\sigma\rho}\epsilon_\mu(k_1)\epsilon_\nu(k_2)k_{1\sigma}k_{2\rho} , \tag{12}$$

where k_1 and k_2 are the four-momenta of the photons. The coupling scale $f_{a\gamma\gamma}$ has the dimensions of mass. The decay rate in the axion's rest frame is

$$\omega_{\gamma\gamma} = \frac{\alpha^2}{8(2\pi)^3}m_a^3\frac{1}{f_{a\gamma\gamma}^2} \approx 0.65/\text{sec} \left[\frac{m_a}{100\text{ keV}}\right]^3$$

$$\times \left[\frac{250\text{ GeV}}{f_{a\gamma\gamma}}\right]^2 . \tag{13}$$

The two-photon coupling depends in detail on the axion coupling to quarks and charged leptons. For the standard axion $f_{a\gamma\gamma}$ can be related by current algebra to the $\pi^0 \to 2\gamma$ width[15]

$$f_{a\gamma\gamma} = f_\phi \frac{\alpha}{8\pi^{3/2}}\frac{m_\pi}{f_\pi}\frac{1+Z}{Z}\frac{1}{N\left|X+\frac{1}{X}\right|}\left[\frac{m_\pi}{\Gamma(\pi^0 \to 2\gamma)}\right]^{1/2}$$

$$= 0.98 f_\phi \frac{1+Z}{Z}\frac{1}{N\left|X+\frac{1}{X}\right|}$$

$$= \frac{124\text{ GeV}}{Z^{1/2}}\left[\frac{100\text{ keV}}{m_a}\right] \tag{14}$$

using Eq. (9). Thus, the standard axion $a \to \gamma\gamma$ mean lifetime can be written

$$\tau_{a\to\gamma\gamma} = \frac{0.38}{Z}\left[\frac{100\text{ keV}}{m_a}\right]^5 . \tag{15}$$

The Primakoff amplitude [Fig. 4(b)] is governed by the same $a \to \gamma\gamma$ vertex. We treat the nucleus as infinitely heavy and retain only interactions with the nuclear charge density. The Primakoff photoproduction cross section in the nuclear rest frame is

$$\frac{d\sigma}{d\Omega} = \frac{2Z^2\alpha^3}{(2\pi)^3}\frac{1}{f_{a\gamma\gamma}^2}\frac{\beta\sin^2\theta}{(1+\beta^2-2\beta\cos\theta)^2}$$

$$\xrightarrow[m_a\to 0]{} \frac{Z^2\alpha^3}{2(2\pi)^3}\frac{1}{f_{a\gamma\gamma}^2}\frac{1+\cos\theta}{1-\cos\theta} , \tag{16}$$
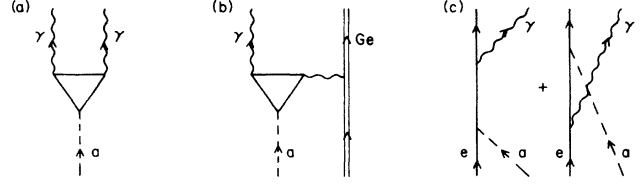

FIG. 4. Diagrams of the (a) $a \to \gamma\gamma$, (b) Primakoff conversion, and (c) axion Compton conversion amplitudes.

where $\beta = k_a/\epsilon_a$. The second line above agrees with the $m_a = 0$ result derived by Barshay *et al.*[16] The total cross section is

$$\sigma = \frac{Z^2\alpha^3}{2\pi^2}\frac{1}{f_{a\gamma\gamma}^2}\frac{1}{\beta}\left[\frac{1+\beta^2}{2\beta}\ln\left|\frac{1+\beta}{1-\beta}\right| - 1\right] , \tag{17a}$$

a result that can be written in terms of $\Gamma(a \to \gamma\gamma)$:

$$\sigma = 32\pi\frac{Z^2\alpha}{m_a^2}\frac{\Gamma(a\to\gamma\gamma)}{m_a}\frac{1}{\beta}\left[\frac{1+\beta^2}{2\beta}\ln\left|\frac{1+\beta}{1-\beta}\right| - 1\right] . \tag{17b}$$

As mentioned above, the forward peaking of the Primakoff cross section, apparent from Eq. (16), renders atomic-screening corrections important even when m_a is an order of magnitude larger than the inverse atomic size. We estimate these corrections in a simple but plausible way. The nuclear vertex is replaced by

$$Ze \to Ze\left[1 - \int_0^\infty r^2 dr\, \rho_e(r)j_0(qr)\right] , \tag{18}$$

where q is the three-momentum transfer to the atom and $\rho_e(r)$ is the atomic charge density (normalized to unity). We assume a simple Gaussian distribution

$$\rho_e(r) \sim e^{-(r/r_0)^2} .$$

The scale parameter r_0 can be determined from the rms atomic radius $\langle r^2\rangle^{1/2} = \sqrt{3/2}r_0$. Equation (18) can be evaluated for this choice of $\rho_e(r)$, yielding

$$Ze \to Ze(1 - e^{-q^2r_0^2/4}) = Ze(1 - e^{q^2\langle r^2\rangle/6}) . \tag{19}$$

It is a straightforward but somewhat tedious task to evaluate the Primakoff cross section with this choice for the atomic charge form factor. For the 1115-keV ^{65}Cu decay screening corrections are important only for $m_a \ll \epsilon_a$, so we can simplify the general result by taking the relativistic limit. In addition, as $\epsilon_a r_0 \gg 1$, we have allowed this parameter $\to \infty$. The ratio of the screened to unscreened cross sections is then given by

$$\chi = \frac{2\ln(2\epsilon_a/m_a) - 1 + e^{-x}(1 - e^{-x}/2) + (x+\frac{1}{2})E_1(2x) - (1+x)E_1(x)}{2\ln(2\epsilon_a/m_a) - 1} , \tag{20}$$

TABLE II. Atomic-screening corrections calculated according to Eq. (20) for an axion energy $\omega_a = 1115$ keV. The parameter r_0 has been equated to the Goldschmidt radii of Ge (1 Å) and Pb (1.75 Å).

m_a (keV)	χ (Ge)	χ (Pb)
100	0.999	1.000
90	0.996	0.999
80	0.989	0.996
70	0.974	0.988
60	0.948	0.969
50	0.911	0.937
40	0.861	0.891
30	0.800	0.829
20	0.724	0.752
10	0.622	0.646
5	0.545	0.566
1	0.424	0.440

where $x = (r_0 m_a^2/4\epsilon_a)^2$ and $E_1(x) = \int_x^\infty (e^{-t}/t)dt$. This parameter, given for various choices for m_a in Table II, then multiplies Eq. (17) to yield our final result. The resulting Primakoff process cross sections for an axion with $\epsilon_a = 1115$ keV are given in Fig. 5 as a function of m_a.

B. Axion Compton cross section

The coupling of the axion to the electron is governed by the Lagrangian

$$\mathcal{L} = i g_{aee} \bar\psi_e \gamma_5 \psi_e \phi_a . \qquad (21)$$

In the standard model the axion-electron coupling is determined by the Peccei-Quinn scale f_ϕ:

$$g_{aee} = \frac{m}{f_\phi} \frac{1}{X} .$$

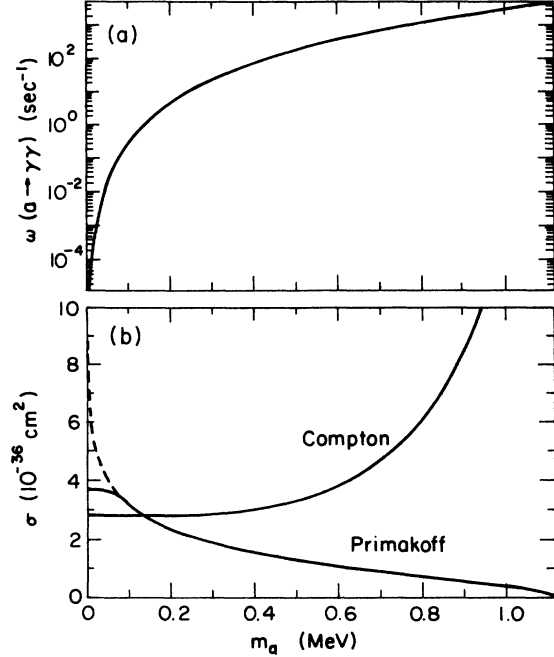The resulting Compton differential cross section in the rest frame of the initial electron is

FIG. 5. The laboratory $a \rightarrow \gamma\gamma$ rate for a 1115-keV axion (a) and Ge Primakoff and electron Compton conversion cross sections (b) are given as a function of m_a. For definiteness, we set all couplings to the values they would have in the standard axion model with $X = 1$ and $f_\phi = 250$ GeV. The axion mass is then varied while these couplings are held fixed. The dashed curve gives the Primakoff cross section when atomic screening corrections are turned off.

$$\frac{d\sigma}{d\Omega} = \frac{\alpha\alpha_a}{2m^2} \frac{\epsilon_\gamma}{k_a} \left\{ 1 + \frac{4m^2\epsilon_\gamma^2}{y^2} - \frac{4m\epsilon_\gamma}{y} - \frac{4m_a^2 k_a^2 m \epsilon_\gamma}{y^3}\sin^2\theta \right\} , \qquad (22)$$

where $\alpha_a = g_{aee}^2/4\pi$, $y = 2m\epsilon_a + m_a^2$, $\epsilon_\gamma = y/2(m + \epsilon_a - k_a\cos\theta)$, and θ is the angle between the axion and emitted photon. The total cross section is

$$\sigma = \frac{\pi\alpha\alpha_a}{2m^2 k_a} \left[\frac{2m^2(m+\epsilon_a)y}{(m^2+y)^2} + \frac{4m(m_a^4 + 2m_a^2 m^2 - 4m^2\epsilon_a^2)}{y(m^2+y)} + \frac{(4m^2 k_a^2 + m_a^4)}{k_a y}\ln\left| \frac{m+\epsilon_a+k_a}{m+\epsilon_a-k_a} \right| \right]$$

$$\xrightarrow[m_a \to 0]{} \frac{\pi\alpha\alpha_a}{m^2}\left[\frac{m}{\epsilon_2}\ln\left| 1 + 2\frac{\epsilon_a}{m} \right| - 2\frac{1+3\epsilon_a/m}{(1+2\epsilon_a/m)^2} \right] . \qquad (23)$$

These results agree with those given by Zhitnitskii and Skorpen.[17] The $m_a = 0$ result of Donnelly et al.[10] is a factor of 2 larger. The Compton cross sections for a 1115-keV axion are given in Fig. 5 as a function of m_a.

VI. RESULTS AND CONCLUSIONS

In this section we present the limits on the axion mass and couplings that we have obtained from our two experiments. For the standard axion, the coupling limits constrain the PQ scale f_ϕ and the ratio X of Higgs-field

expectation values. (We set the number of quark doublets $N = 3$ and use $Z = m_u/m_d = 0.56$.) However, most recent studies of the Peccei-Quinn mechanism have focused on models with nonstandard axion couplings. In such models the couplings of axions to nucleons, electrons, and photons may vary significantly from standard-model values. Thus we also consider the general constraints imposed by our experiments on pseudoscalars that couple to the nucleon and to either the electron or two photons.

A. Results for the Ge experiment

The pulse-height spectrum for the Ge detector is shown in Fig. 6. The full energy spectrum is a typical spectrum acquired in 17 days of running. The inserted partial spectrum near the expected line at 1115 keV represents the total data obtained in 295 days. These data were analyzed for a peak at 1115 keV using a maximum-likelihood analysis. The upper limit for the experimental rate is 1.1 (1.6) events per day at the 1σ (3σ) confidence level.

The calculation of the expected single-photon rate includes two processes discussed previously, Compton production off electrons in the detector and the Primakoff production off the Ge nuclei. The produced gamma rays then interact with the detector. The efficiency of detection of the secondary gamma rays is estimated by standard methods. In addition, Primakoff conversion can produce 1115-keV photons in the lead surrounding the detector. These gamma rays are attenuated by the lead, but some of them penetrate into the Ge detector without interacting with the lead.

The rate of detection of axions that convert in the Ge detector can be expressed as

$$R = \sigma N_0 \langle \phi_a \rangle V \epsilon ,\qquad (24)$$

where σ is the cross section for either Primakoff or Compton conversion, $\langle \phi_a \rangle$ is the axion flux, V is the volume of the Ge detector (145 cm^3), and ϵ is the efficiency of the detector for totally absorbing the energy of the 1115-keV axion. The efficiency depends on the geometry of the photon production process, and thus differs for the Primakoff and Compton processes. A Monte Carlo code developed earlier by one of us was used to determine $\epsilon_{\text{Compton}} = 0.35$ and $\epsilon_{\text{Primakoff}} = 0.17$. For the Primakoff process, N_0 is the density of Ge atoms in the detector, 4.5×10^{22} atoms/cm.^{2} For Compton

FIG. 6. Typical Ge spectrum comprising 17 d of data taking. The inset shows the total counts near 1115 keV in 295 d of data taking.

scattering, this number is multiplied by $Z = 32$ to give the number of electrons in the detector. $\langle \phi_a \rangle$ is the average axion flux, given by

$$\langle \phi_a \rangle = \langle \phi_\gamma \rangle \frac{\omega_a}{\omega_r} \langle \epsilon' \rangle ,\qquad (25)$$

where $\langle \phi_\gamma \rangle$ is the flux of photons from ^{65}Cu that would have arrived at the detector had there been no intervening material, and ω_a / ω_r is the axion-to-photon–decay rate ratio, given by Eq. (10). Our estimate of $\langle \phi_\gamma \rangle$ is based on an average effective source strength. The activity of the source, initially measured at 40.8 kCi, diminished during the course of our experiment in accordance with the 245-day half-life of ^{65}Zn. The effective activity was calculated for the periods during which data were taken, for a total of 295 days. ϕ_γ also depends on the distance between source and detector. Two distances were used, 74.93 cm (before mounting on wheels) and 101.85 cm (after mounting on wheels). Of course, the activity of the source differed for these two positions. Averaging over position and time, we find an effective $\langle \phi_\gamma \rangle = 2.15 \times 10^9$ photons/cm^2 sec over the 295-d experiment. Finally $\langle \epsilon' \rangle$ is the probability that an axion produced in the source will not decay in transit to the detector. For axions with $m_a < 2m_e$ that couple weakly to the electron and two photons, one can assume $\langle \epsilon' \rangle = 1$. Otherwise, as we discuss below, $\langle \epsilon' \rangle$ depends on these couplings, the axion mass, and the position of the detector.

Compton production in the lead shield generally results in some deposition of energy in the lead due to electron recoil. In contrast, Primakoff conversion in the shield can generate a 1115-keV photon that arrives at the detector while still carrying the entire decay energy. An estimate of this contribution is complicated by the need to account for the absorption and scattering in the lead and the nontrivial geometry. A Monte Carlo calculation showed that a slightly underestimated rate is obtained by assuming that the only axions that contribute to the rate are those that traverse a parallelopiped, the dimensions of which are the diameter and height of the detector. As the axion cross sections are small, the γ-ray production rate is constant throughout the transit. We assume that any interaction of the γ rays with the lead degrades them sufficiently that they do not produce a ~ 1115-keV signal in the detector. We can write the expression for this rate as

$$R^{\text{Pb}}_{\text{Primakoff}} = \sigma N_0 \langle \phi_a \rangle \frac{DL}{\mu} \epsilon ,\qquad (26)$$

where σ is the Primakoff cross section for lead, N_0 is the density of Pb atoms/cm^3, μ is the total γ-ray attenuation of Pb for 1115-keV γ rays (in cm^{-1}), D and L are the diameter and length of the Ge crystal, respectively, and ϵ is the probability that the 1115-keV γ ray will deposit all of its energy in the Ge detector. Our Monte Carlo calculations yielded $\epsilon = 0.096$.

The constraints imposed by the Ge experiment on the standard axion model are shown in Fig. 7 as a function of the Peccei-Quinn scale f_ϕ and the ratio X of expecta-
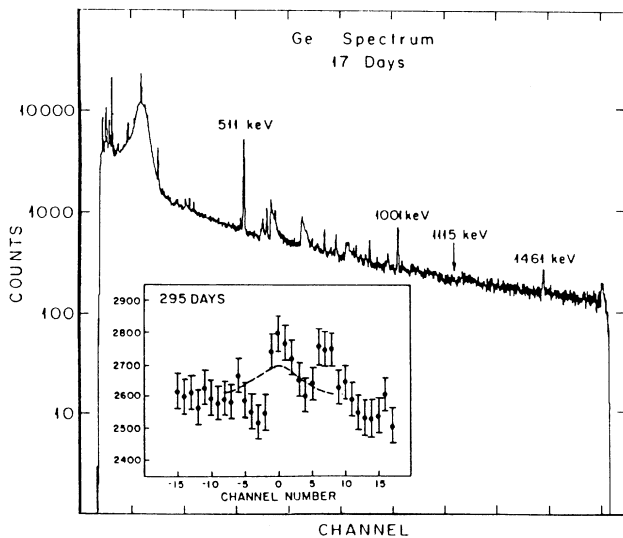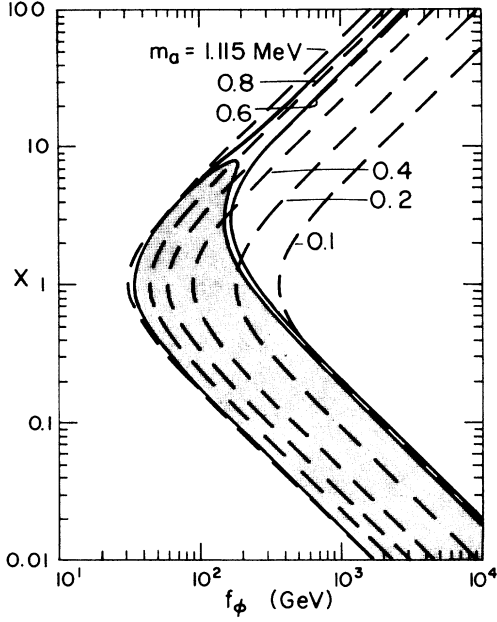
FIG. 7. For the standard-axion model, the shaded region indicates those values of f_ϕ and X that are ruled out by the Ge experiment at the 3σ confidence level. The encircling contour gives the 1σ limits. The dashed lines are contours of constant m_a.
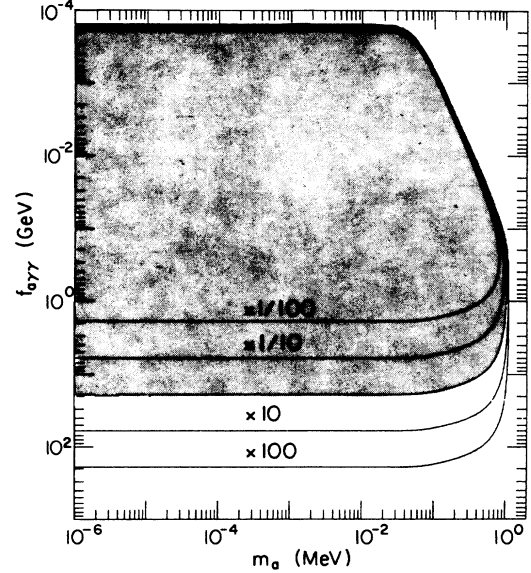
FIG. 8. General limits imposed by the Ge experiment on $f_{a\gamma\gamma}$ are given as a function of m_a. In the middle contour we have taken $(1.81g^0_{aNN}+g^1_{aNN})^2=0.014$, the standard-axion value for $X=1$ and $f_\phi=250$ GeV. This value is scaled as indicated to give the other contours. Note that large values of $f_{a\gamma\gamma}$ correspond to weak $a\rightarrow\gamma\gamma$ couplings.

tion values of the Higgs fields. The shaded region represents those values excluded by the 3σ limit on the counting rate, 1.6 per day. The encircling contour corresponds to the 1σ limit, 1.1 per day. The dashed lines are the contours of constant m_a. The kinematic constraints of our experiment (a total decay energy of 1115 keV) permit us to probe only that part of the f_ϕ-X plane to the right of the $m_a=1115$-keV contour.

Below $X\sim0.4$ we exclude all standard axions in the mass range of approximately $2m_e\gtrsim m_a\gtrsim100$ keV. (Axions much above $2m_e$ in mass have a high probability of decaying into e^+e^- before they reach the detector, thus generating a small value for $\langle\epsilon'\rangle$.) For larger X we begin to lose sensitivity to axions of low mass as g_{aee}, which is proportional to $1/X$, weakens. Above $X=8$ no constraints are obtained at the 3σ confidence level. For very large X we do rule out axions in the mass range $650\gtrsim m_a\gtrsim850$ at the 1σ confidence level because of the contribution of the Primakoff conversion process to the counting rate. However, above 850 keV (below 650 keV) the decreasing Primakoff process phase space (decreasing strength of the $a\rightarrow\gamma\gamma$ coupling) prevents us from constraining X and f_ϕ even at the 1σ level.

In Fig. 8 we present the general (i.e., valid for general models incorporating axions) constraints that this experiment can place on light pseudoscalars that couple to the nucleon and to two photons ($g_{aee}=0$). The shaded region indicates those values of m_a and $f_{a\gamma\gamma}$ that are ruled out at the 3σ level, given that the nuclear coupling $(1.81g^0_{aNN}+g^1_{aNN})^2=0.014$, the standard-axion value for

$X=1$ and $f_\phi=250$ GeV. The other contours correspond to fixing $(1.81g^0_{aNN}+g^1_{aNN})^2$ at $\frac{1}{100}$, $\frac{1}{10}$, 10, and 100 times this value. (One can thus easily scale the excluded region for any choice of g^0_{aNN} and g^1_{aNN}.)

The lower bound of the excluded region is a horizontal line for $0\lesssim m_a\lesssim50$ keV, reflecting the constant phase space for the Primakoff process for such masses (a result of the atomic screening). From 50 to 1115 keV the contours bend gently toward the vertical: the loss of sensitivity to small $f_{a\gamma\gamma}$ reflects the phase-space effects that diminish both the Primakoff cross section and the ω_a/ω_γ nuclear branching ratio. For values of $f_{a\gamma\gamma}$ below 0.1 GeV the contours bend inward: heavy axions decay to two photons before they reach the detector. One retains sensitivity to light axions because of the Lorentz dilation of the laboratory $a\rightarrow\gamma\gamma$ decay lifetime. However, for very strong couplings ($f_{a\gamma\gamma}\sim0.2$ MeV), all light axions will convert by Primakoff scattering in the lead shielding, leading to the horizontal upper boundary for the shaded region in Fig. 8.

The analogous general constraints for light pseudoscalars that couple to the nucleon and the electron are given in Fig. 9. The contours for small g_{aee} and large m_a are much more square than in Fig. 8 because the increasing Compton phase space compensates for the decreasing nuclear branching ratio ω_a/ω_γ as m_a approaches $2m_e$. The upper boundary of the shaded region ($g_{aee}\sim0.5$) is imposed by the almost complete absorption of axions due to Compton scattering in the lead surrounding the source and detector.
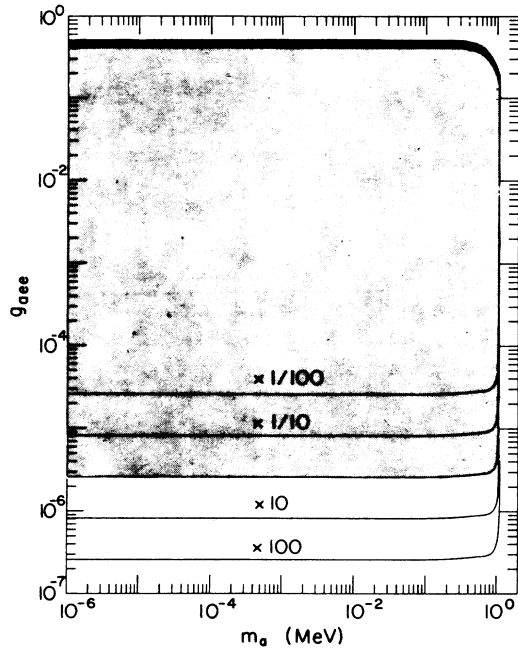
FIG. 9. As in Fig. 8, only for g_{aee}.

B. Results for the NaI(Tl) coincidence experiment

A typical sum spectrum for the coincidences in two NaI detectors is illustrated in Fig. 10. There is a broad, continuous background due to cosmic rays and natural radioactivity in the lead shielding with a cutoff of about 250 keV, but no evidence for a peak at 1115 keV. We combine the data for coincidences involving any two detectors. (We have six pairs, four on adjoining corners and two on the diagonals.) In addition, by measuring separately with a calibration source, we determine that our Apple II computer acquisition system recorded only 30% of the true events. Thus we divide our measured coincidence rate by 0.3 to determine a corrected "experimental" value of

$$R_{\gamma\gamma} = 28 \pm 10 \text{ coincidences/d}$$

for the number of coincidences summed over all six detector pairs. This result is not significantly different from zero. At the 3σ level, the upper limit for the rate is then $R_{\gamma\gamma} < 62$ coin per day. This can be compared to the result of Lehmann *et al.*, who achieved a lower counting rate, $R_{\gamma} < 5.4$ coin per day (95% C.L.),[7] but used a source that was about six times weaker than ours. The geometry of that experiment also differed because of the longer decay path. As we discuss later in this section, the present experiment is more sensitive to axions with $m_a \geq 225$ keV.

The theoretical rate that we compare to our limit $R_{\gamma\gamma} < 62$ coin per day (3σ) depends on the axion flux, the solid angle intercepted by our detector array, and the probability that an axion decays in the 40-cm decay region, generating a coincidence in two of the detectors.
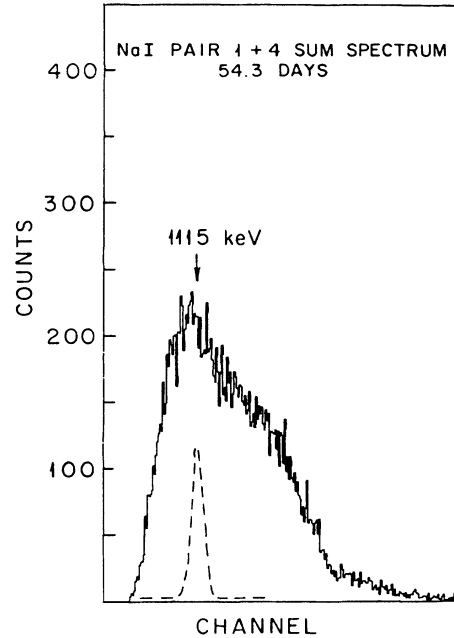
FIG. 10. Typical sum spectrum for one pair of NaI detectors. The dotted curve indicates the shape and size of the 1115-keV peak for an axion decay yielding 2.6×10^{-4} coincidences/sec per pair, the rate that would be expected for $f_\phi = 230$ GeV and $X = 1$ ($m_a \sim 157$ keV).

Thus we have to fold the geometry of the decay with the geometry of the detector system, which we have done with a Monte Carlo code. In particular, note that the opening angle between the photons, $\theta = 2 \arccos(1 - m_a^2/\epsilon_a^2)^{1/2}$, is a sharply varying function of m_a. Because the minimum separation between our
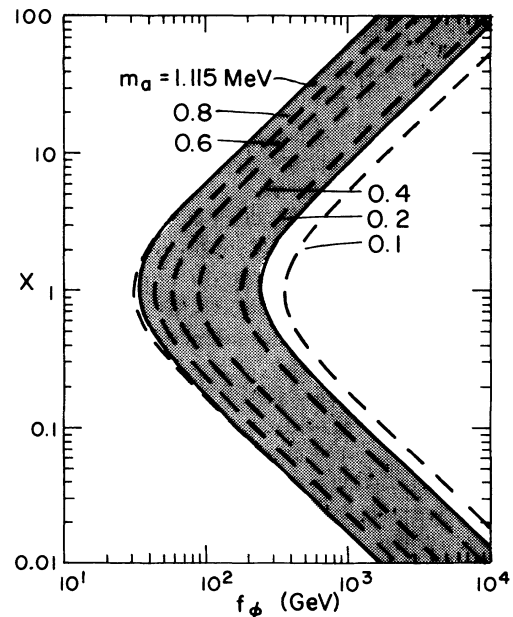

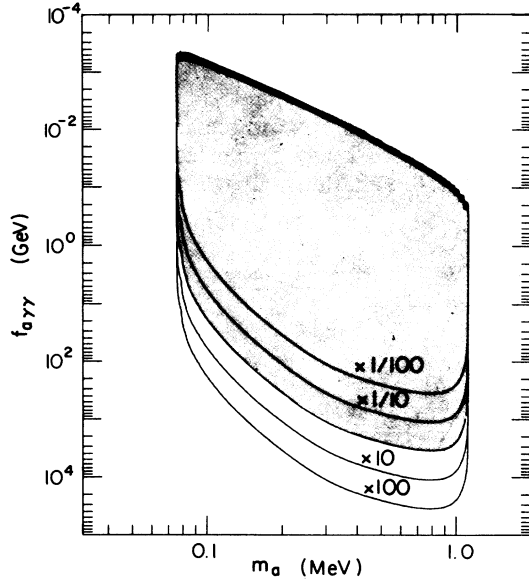FIG. 11. As in Fig. 7, only for the 3σ confidence limits of the NaI experiment.

FIG. 12. General limits imposed by the NaI experiment on $f_{a\gamma\gamma}$ are given as a function of m_a. The contours are labeled as in Fig. 8.
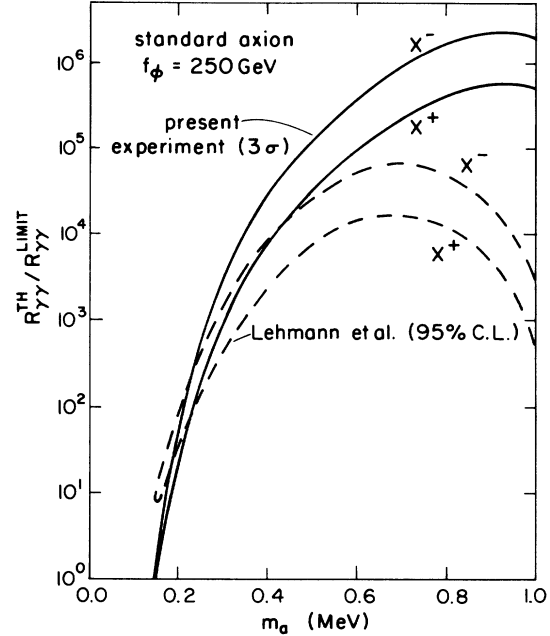

FIG. 13. Comparison of the sensitivities of the present and Lehmann et al. experiments. The ratios of the standard axion theoretical rates to the respective counting-rate limits are given for the two values of X corresponding to each m_a.

detectors is 5 cm, the 40-cm decay path prevents us from detecting axions with $m_a \lesssim 80$ keV. In addition, in the case of strongly coupled nonstandard axions, we take into account all axions decays or interactions in the lead shielding that would reduce the effective flux at the detectors.

In Fig. 11 the constraints imposed by the coincidence experiment on the standard-axion model are given as a function of f_ϕ and X, with the contours defined as in Fig. 7. The shaded region represents those values excluded by our 3σ limit, 62 coincidences per day. For small X, axions with $2m_e \gtrsim m_a \gtrsim 150$ keV are ruled out at the 3σ confidence level. The excluded region is slightly narrower than that of Fig. 7, where axions as light as 100 keV were excluded. However for large X, where the Ge experiment imposed only very weak constraints on the standard model, the excluded region remains broad. These results thus nicely complement those of Fig. 7. Note that the coincidence experiment excludes all axions with $m_a \lesssim 2m_e$ and with $f_\phi \lesssim 240$ GeV, independent of the value of X.

In Fig. 12 we present the general constraints this experiment places on light pseudoscalars that couple to the nucleon and two photons ($g_{aee} = 0$). The shaded region is again ruled out at the 3σ confidence level. The left and right boundaries of that region are imposed by the kinematics of the ^{65}Cu decay ($m_a \lesssim 1115$ keV) and by the detector geometry ($m_a \gtrsim 80$ keV, as discussed above). For $m_a \gtrsim 100$ keV, the NaI experiment is sensitive to larger $f_{a\gamma\gamma}$ (that is, weaker $a \rightarrow \gamma\gamma$ couplings) than those probed in the Ge experiment, and the difference in sensitivity becomes quite significant for heavier axions.

To compare our results with those of Lehmann et al.,[7] in Fig. 13 we plot the ratio of the standard-axion theoretical rates for these experiments to the respective

counting-rate limits. A fixed $f_\phi = 250$ GeV was chosen. Two values of X are permitted for each value of m_a [see Eq. (9)]. The curves corresponding to the larger and smaller are labeled by X^+ and X^-, respectively. Note that the present experiment is more sensitive to axions with $m_a \geq 225$ keV, but that the earlier experiment provides the more stringent limit on lighter axions. The results of Ref. 7 have been replotted for the ω_a/ω_γ ratio of Eq. (11). (The expression for ω_a/ω_γ used in Ref. 7 is only appropriate for a single-proton $p_{3/2} \leftrightarrow p_{1/2}$ transition. Based on our shell-model work, this overestimates the ^{65}Cu axion decay rate by about an order of magnitude.)

We stress that all of the results in this section are subject to some uncertainty in the theoretical prediction of the axion/γ branching ratio. This enters, effectively, as an uncertainty in the coefficients of g_{aNN}^0 and g_{aNN}^1 in the expression $(1.81 g_{aNN}^0 + g_{aNN}^1)$, as discussed in Sec. IV.

C. Conclusions

We have placed rather general constrains on axion parameters by combining two experiments. In particular, the Ge experiment permitted us to probe very light axions whose couplings to $\gamma\gamma$ and to electrons are similar in strength to those of the standard axion if f_ϕ is near the weak scale ($f_\phi \sim 250$ GeV). This is a unique result in searches for axions in nuclear transitions.

*Present address: Argonne National Laboratory, Argonne, IL 60439.

†Present address: Lawrence Berkeley Laboratory, Berkeley, CA 94720.

[1]F. D. Peccei and H. R. Quinn, Phys. Rev. Lett. **38**, 1440 (1977); Phys. Rev. D **16**, 1791 (1977).

[2]S. Weinberg, Phys. Rev. Lett. **40**, 223 (1978); F. Wilczek, *ibid.* **40**, 279 (1978).

[3]M. Dine, W. Fischler, and M. Srednicki, Phys. Lett. **104B**, 199 (1981); J. Preskill, M. B. Wise, and F. Wilczek, *ibid.* **120B**, 127 (1983); L. F. Abbott and P. Sikivie, *ibid.* **120B**, 133 (1983); M. Dine and W. Fischler, *ibid.* **120B**, 137 (1983); N. Iwamoto, Phys. Rev. Lett. **53**, 1198 (1984); D. A. Dicus, E. W. Kolb, V. L. Teplitz, and R. V. Wagoner, Phys. Rev. D **18**, 1829 (1978); M. Fukugita, S. Watamure, and M. Yoshimura, Phys. Rev. Lett. **48**, 1588 (1982); L. Krauss, J. Moody, and F. Wilczek, Phys. Lett. **144B**, 391 (1984).

[4]D. Kaplan, Nucl. Phys. **B260**, 215 (1985), and references therein.

[5]T. Cowan *et al.*, Phys. Rev. Lett. **54**, 761 (1985); R. D. Peccei, T. T. Wu, and T. Yanagida, Phys. Lett. **172B**, 435 (1986); L. M. Krauss and F. Wilczek, *ibid.* **173B**, 189 (1986).

[6]A. L. Hallin, F. P. Calaprice, R. W. Dunford, and A. B. McDonald, Phys. Rev. Lett. **57**, 2105 (1986); E. Warburton *et al.*, Phys. Rev. **133**, B42 (1964).

[7]P. Lehmann, E. Lesquoy, A. Muller, and S. Zylberajch, Phys. Lett. **115B**, 270 (1982).

[8]F. T. Avignone III, R. L. Brodzinski, D. P. Brown, J. C. Evans, Jr., W. K. Hensley, H. S. Miley, and J. H. Reeves, Phys. Rev. C **34**, 666 (1986).

[9]R. T. Kouzes, L. Piilonen, and D. Schreiber, Nucl. Sci. **30**, 3895 (1983).

[10]T. W. Donnelly, S. J. Freedman, R. S. Lytel, R. D. Peccei, and M. Schwartz, Phys. Rev. D **18**, 1607 (1978).

[11]R. L. Auble, Nucl. Data Sheets **16**, 351 (1973).

[12]F. R. Metzger, Phys. Rev. **171**, 1257 (1968).

[13]T. T. S. Kuo and G. E. Brown, Nucl. Phys. **A114**, 241 (1968).

[14]A. Oberstedt, D. Bohle, G. Kückler, A. Richter, E. Spamer, and C. Rangacharyulu, Technische Hochschule Darmstadt report, 1986 (unpublished).

[15]W. A. Bardeen and S.-H. H. Tye, Phys. Lett. **74B**, 229 (1978).

[16]S. Barshay, H. Faissner, R. Rodenberg, and H. de Witt, Phys. Rev. Lett. **46**, 1361 (1981).

[17]A. R. Zhitnitskii and Yu. I. Skorpen, Yad. Fiz. **29**, 995 (1979) [Sov. J. Nucl. Phys. **29**, 513 (1979)].
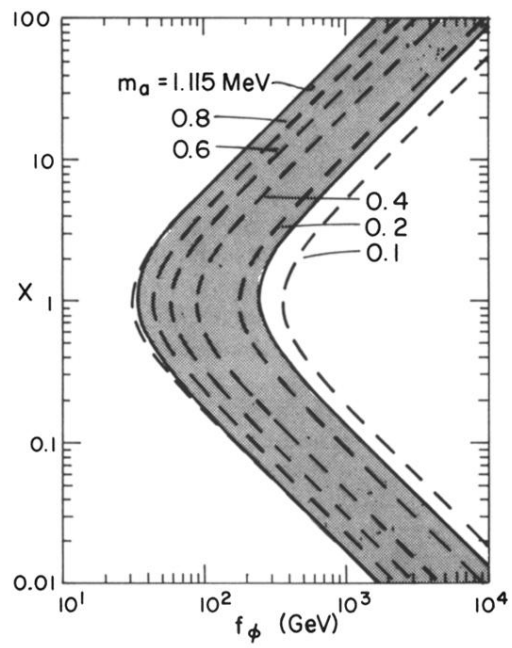
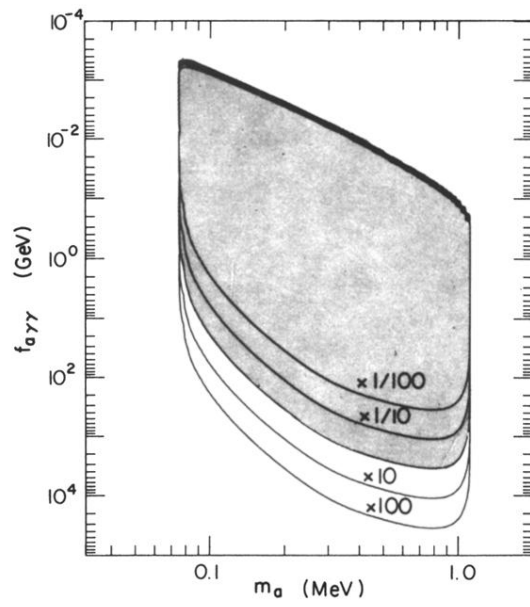FIG. 11. As in Fig. 7, only for the 3σ confidence limits of the NaI experiment.

FIG. 12. General limits imposed by the NaI experiment on $f_{a\gamma\gamma}$ are given as a function of m_a. The contours are labeled as in Fig. 8.
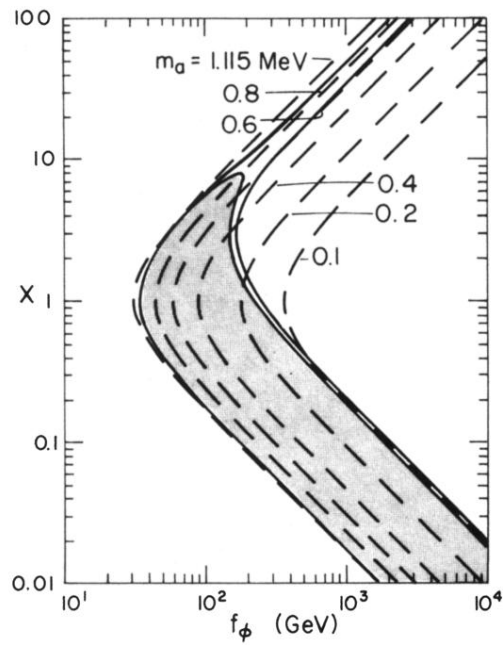
FIG. 7. For the standard-axion model, the shaded region indicates those values of f_ϕ and X that are ruled out by the Ge experiment at the 3σ confidence level. The encircling contour gives the 1σ limits. The dashed lines are contours of constant m_a.
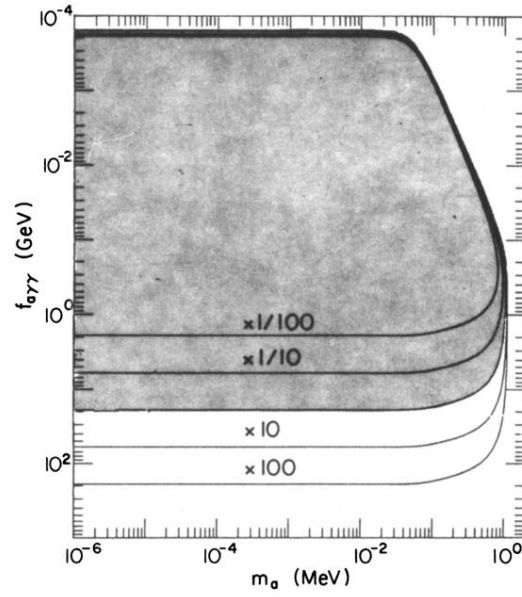
FIG. 8. General limits imposed by the Ge experiment on $f_{a\gamma\gamma}$ are given as a function of m_a. In the middle contour we have taken $(1.81g_{aNN}^0 + g_{aNN}^1)^2 = 0.014$, the standard-axion value for $X = 1$ and $f_\phi = 250$ GeV. This value is scaled as indicated to give the other contours. Note that large values of $f_{a\gamma\gamma}$ correspond to weak $a \rightarrow \gamma\gamma$ couplings.
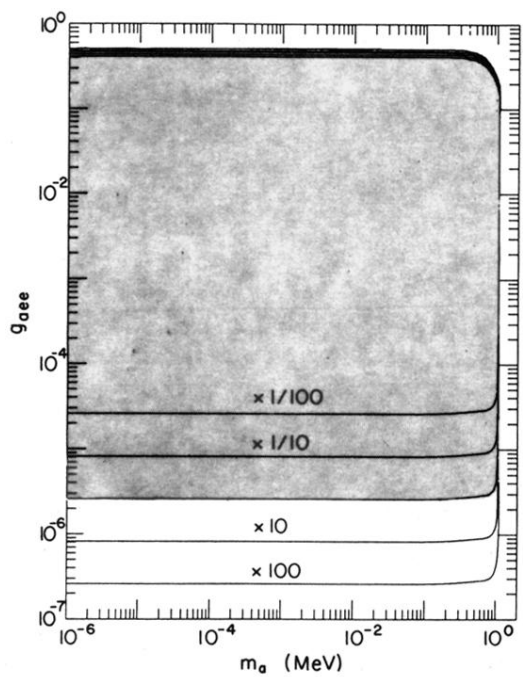
FIG. 9. As in Fig. 8, only for g_{aee}.